ACS APPLIED MATERIALS & INTERFACES

Research Article

www.acsami.org

Pt- and Ru-Doped SnO_2–Sb Anodes with High Stability in Alkaline Medium

Raúl Berenguer,[†] Juan Manuel Sieben,[‡] César Quijada,[§] and Emilia Morallón*[,∥]

[†]Andalucía Tech, Departamento de Ingeniería Química, Universidad de Málaga, 29071 Málaga, Spain

[‡]Instituto de Ingeniería Electroquímica y Corrosión and CONICET, Universidad Nacional del Sur, Avenida Alem 1253, B8000CPB Bahía Blanca, Argentina

[§]Departamento de Ingeniería Textil y Papelera, ~~Universidad Politécnica~~ de ~~Valencia~~, Plaza de Ferrándiz y Carbonell, E-03801 Alcoy (Alicante), Spain

[∥]Departamento de Química Física e Instituto Universitario de Materiales, Universidad de Alicante, Apartado 99, E-03080 Alicante, Spain

Supporting Information

ABSTRACT: Different Pt- and Ru-doped Ti/SnO_2–Sb electrodes were synthesized by thermal decomposition. The effect of the gradual substitution of Sb by Ru in the nominal composition on the physicochemical and electrochemical properties were evaluated. The electrochemical stability of the electrodes was estimated from accelerated tests at 0.5 A g^{-1} in 1 M NaOH. Both as-synthesized and deactivated electrodes were thoroughly characterized by scanning electron microscopy (SEM), energy-dispersive X-ray microanalysis (EDX), transmission electron microscopy (TEM), X-ray photoelectron spectroscopy (XPS) and X-ray diffraction analysis (XRD). The incorporation of a small amount (about 3 at. %) of both Pt and Ru into the SnO_2–Sb electrodes produced a 400-times increase in their service life in alkaline medium, with no remarkable change in the electrocatalysis of the oxygen evolution reaction (OER). It is concluded that the deactivation of the electrodes is promoted by alkaline dissolution of metal species and coating detachment at high potentials. The introduction of Pt has a coating compacting effect, and Ru(IV), at low amounts until 9.75 at. %, replaces the Sn(IV) cations in the rutile-like SnO_2 structure to form a solid solution that strongly increases the stability of the electrodes. The observed Ru segregation and decreased stability for larger Ru contents (x > 9.75 at. %), together with the selective dissolution of Ru after deactivation, suggest that the formation of a homogeneous $(Ru_\delta Sn_{1-\delta})O_2$ single-phase is crucial for the stabilization of these electrodes.

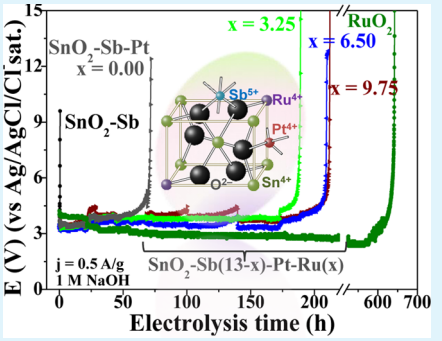

KEYWORDS: *DSA electrodes, doped tin dioxide electrodes, electrochemical stability, ruthenium oxide, alkaline solutions*

1. INTRODUCTION

Because of their unique properties and extremely high versatility, transition metal oxides (TMOs) have received a great interest as electrodes in many electrochemical applications.[1−17] Thus, they have been widely used in the chlor-alkali industry,[2] and multiple processes using electrolyzers,[2−4] and constitute promising electrode materials for more sustainable and environmentally friendly technologies in water remediation[5−12] and energy storage and conversion.[13−16] Apart from a suitable performance, the economics and feasibility of the TMOs electrodes in these applications largely depend on their service life at operation conditions.[1,17]

The tremendous success of some active TMOs (RuO_2, IrO_2, Co_3O_4, etc.) supported onto a Ti substrate (the so-called dimensionally stable anodes, DSA), can be associated with their high stability and long lifetime at high potentials in aqueous electrolytes, where the oxygen evolution reaction (OER) occurs, as well as their good catalytic activity for this reaction, what provide lower cell-voltages and better faradic efficiencies in multiple processes.[1,2,17] Nevertheless, for some applications, such as the electrochemical degradation of pollutants in wastewater,[5−12] the electrodes should have not only a good stability but also a high overpotential for the OER side-reaction.

The composition and the nature of the oxide coating strongly affect the stability and electrochemical activity of these DSA electrodes.[1,17−19] Because of their high OER overpotential, considerably lower cost and innocuous character, the Sb-doped SnO_2 electrodes[20−22] have been found to be, among different choices, the most promising alternatives to the more expensive and fragile Boron-Doped Diamond (BDD) electrodes,[12,23,24] and the more harmful, lead-leaching, PbO_2-based electrodes.[25] Unfortunately, their anodic stability is remarkably low.[20,21,26,27]

Although different approaches have been proposed to increase the stability of the SnO_2–based electrodes, most of

Received: October 9, 2014
Accepted: December 2, 2014

   dx.doi.org/10.1021/am506958k | ACS Appl. Mater. Interfaces XXXX, XXX, XXX–XXX

them focused on acid electrolytes,[21,28−30] whereas the stability enhancement in alkaline medium has received less attention.[31] In general, the combination of SnO_2-based electrodes with active species (Pt, Ir, Ru) enhances their stability, but it simultaneously increases the catalytic activity toward the OER and the cost of the electrodes; however, the optimization of the amount of active metal has not been often considered.[5−12] In addition, these investigations mainly determined the service life of the electrodes without deepening into a detailed characterization of fresh and deactivated electrodes. So the understanding of the stabilization effect and the deactivation mechanisms need further research.

Considering the growing application of electrochemistry in different fields, the development of high-performance electrodes for alkaline electrolytes gathering both high OER-overpotential and stability, is very interesting for multiple electrochemical applications, such as fuel cells, electro-oxidation of compounds in electrosynthesis or the electrochemical degradation of pollutants, etc.[1−17] For this purpose, the establishment of structure-composition vs stability correlations and the investigation of the deactivation mechanism of the electrodes are of utmost importance to further propose new stabilization strategies.

It has been previously found that the introduction of a small amount (3 at. %) of Pt enhances the service life of Sb-doped SnO_2 electrodes in acidic electrolyte by 2 orders of magnitude,[28] also showing an even higher efficiency for phenol electro-oxidation in the same medium; however, higher amounts of Pt (13 at. %) decrease their performance.[32] On the other hand, it is well-documented that RuO_2 exhibits a high catalytic activity and stability for the OER.[31,33] The stability of binary $(Sn−Ru)O_2$ oxides were previously studied, but experiments were restricted to acidic medium[29,34] and the influence of Sb or Pt was not considered. Consequently, in this work we have investigated the influence of Pt, as well as the progressive substitution of Sb by Ru in the nominal composition of SnO_2−Sb/Ti electrodes, on the physicochemical properties and the electrochemical response of the electrode. For this purpose, different SnO_2−Sb(13−x)-Pt(3)-Ru(x)/Ti electrodes ($0 \le x$ (at. %) ≤ 13), were synthesized by thermal decomposition and thoroughly characterized, before and after deactivation. The electrochemical stability of the electrodes was estimated by accelerated tests at 0.5 A g^{-1} in 1 M NaOH. The structural properties were studied by SEM, TEM and XRD, whereas the chemical composition was followed by EDX and XPS. The electrochemical behavior as well as the catalytic activity toward the OER was analyzed by cyclic voltammetry and Tafel measurements, respectively, in the same electrolyte. Furthermore, SnO_2−Sb/Ti, SnO_2−Ru/Ti, and RuO_2/Ti electrodes were prepared and characterized by the same techniques.

2. EXPERIMENTAL SECTION

Four types of tetragonal rutile-like oxide electrodes (with composition in brackets expressed as metal atomic percentage), SnO_2−Sb(13 at. %), SnO_2−Sb(13−x)−Pt(3)−Ru(x) (with $0 \le x \le 13$ at. %), SnO_2−Ru(13 at. %) and RuO_2, were synthesized by the thermal decomposition method following the procedure described elsewhere.[33] Briefly, the precursor solutions, consisting of $SnCl_4 \bullet 5H_2O$, $SbCl_3$, $H_2PtCl_6 \cdot 6H_2O$ and $RuCl_3 \cdot nH_2O$ in absolute ethanol and HCl with the desired nominal composition, were spread over pretreated Ti plates (1 cm × 1 cm × 0.05 cm; Goodfellow 99.6%) by brushing. Previously, the Ti plates were degrased in acetone, etched in a boiling 10% oxalic acid solution for 1 h and finally rinsed with distilled water. The sample was dried at 70 °C in order to evaporate the solvent and the metal oxides were formed by calcination at 400 °C for 10 min. This procedure was successively repeated to increase the oxide loading up to ca. 1.5−2.0 mg cm^{-2}. The number of deposition steps for these loadings were between 20 and 25. A final annealing step was carried out for 60 min at 600 °C.

The nominal composition of the precursor solution is presented in Table 1. In all cases, the total metal cation concentration was kept constant at 0.5 m.

Table 1. Nominal Composition of the Precursor Solutions for the Different Electrodes

		g of salt precursor/100 g of solution				
electrode	x^a	$SnCl_4 \cdot 5H_2O$	$SbCl_3$	$H_2PtCl_6 \cdot 6H_2O$	$RuCl_3 \cdot nH_2O$	ethanol (mL)
SnO_2−Sb/Ti	0.00	10.000	1.000			112.7
SnO_2−Sb(13−x)−Ru(x)−Pt/Ti	0.00	10.000	1.000	0.400		112.4
	3.25	10.000	0.750	0.400	0.287	112.4
	6.50	10.000	0.500	0.400	0.573	112.3
	9.75	10.000	0.250	0.400	0.860	112.3
	13.00	10.000		0.400	1.146	112.2
SnO_2−Ru/Ti	13.00	10.000			1.146	112.5
Ti/RuO_2/Ti	100				5.186	50.0

^{a}x = nominal Ru percentage.

2.2. Physicochemical Characterization. The surface morphology of the electrodes was studied by scanning electron microscopy (SEM) in a Hitachi S-3000N electron microscope coupled to a Rontec X-ray detector for energy dispersive X-ray (EDX) microanalysis. The microstructure and crystallinity were characterized by X-ray diffraction (XRD) in a KRISTALLOFLEX K 760−80F diffractometer (Bruker D8-Advance) by using a Ni-filtered Cu Kα radiation (λ = 1.5416 Å). Diffraction data points were recorded stepwise within 2θ = 20−80° at a scan rate of 0.03° min^{-1} with a scan step of 0.05° in 2θ. Cell parameters were calculated by a computer program using the peak position obtained after fitting the experimental range with a pseudo-Voigt function per peak plus a background line. Line-broadening analysis was performed to determine the average crystallite size.

The morphology and particle size were analyzed by transmission electron microscope (TEM) in a JEOL equipment (JEM-2010) with an accelerating voltage of 200 keV. X-ray photoelectron spectroscopy (XPS) measurements were carried out by a VG-Microtech Multilab 3000 spectrometer with Mg Kα radiation ($h\nu$ = 1256.3 eV) at base pressure of 5×10^{-10} mbar in the analysis chamber. Binding energies were referenced against the main C(1s) line of adventitious carbon impurities at 284.6 eV. Peak energies were given to an accuracy of 0.2 eV and peak areas were normalized by using appropriate atomic sensitivity factors.

2.3. Electrochemical Measurements. The electrochemical measurements were performed on an Autolab PGSTAT 30 potentiostat controlled by GPES EcoChimie software using a conventional three-electrode glass cell. The counter electrode was a spiral of platinum wire of 12 cm length and 0.5 mm of diameter and the potentials are referred to a reversible hydrogen electrode (RHE) immersed in the same solution. The aqueous 0.1 M NaOH solutions were deoxygenated by N_2 bubbling. All solutions were prepared with purified water obtained from an Elga Labwater Purelab system (18.2 MΩ cm). In these studies, cyclic voltammetry (CV) measurements were performed between different potential limits at a scan rate between 1 and 500 mV s^{-1}. The current densities were calculated using the apparent geometric area of the electrodes (2 cm^2). The voltammetric charges (q^*) corresponding to electrochemically active surface areas were determined by integrating the area of the cyclic voltammograms. The electrocatalytic activity toward OER was investigated in aqueous 0.1 M NaOH solution by galvanostatic experiments at current densities lower than 5 mA cm^{-2} at a scan rate of 3 μA s^{-1}.

dx.doi.org/10.1021/am506958k | ACS Appl. Mater. Interfaces XXXX, XXX, XXX−XXX

The accelerated service-life tests were performed by anodic polarization of the different electrodes at 0.5 A cm^{-2} in a 1 M NaOH solution at a controlled temperature of 25 °C. The anode potential was measured as a function of time, and the electrode was considered to be deactivated when the potential increased to 5 V above its initial value. In these experiments a Ag/AgCl/Cl^-(sat.) electrode served as the reference electrode. The electrolyte composition after the anodic deactivation treatment was determined by ICP-OES analysis (PerkinElmer 7300 DV).

3. RESULTS AND DISCUSSION

3.1. Physicochemical Characterization. *3.1.1. Surface Morphology.* The as-prepared SnO_2–Sb/Ti, RuO_2/Ti and SnO_2–Sb-Pt/Ti electrodes (Figure 1a,c,e, respectively) exhibit

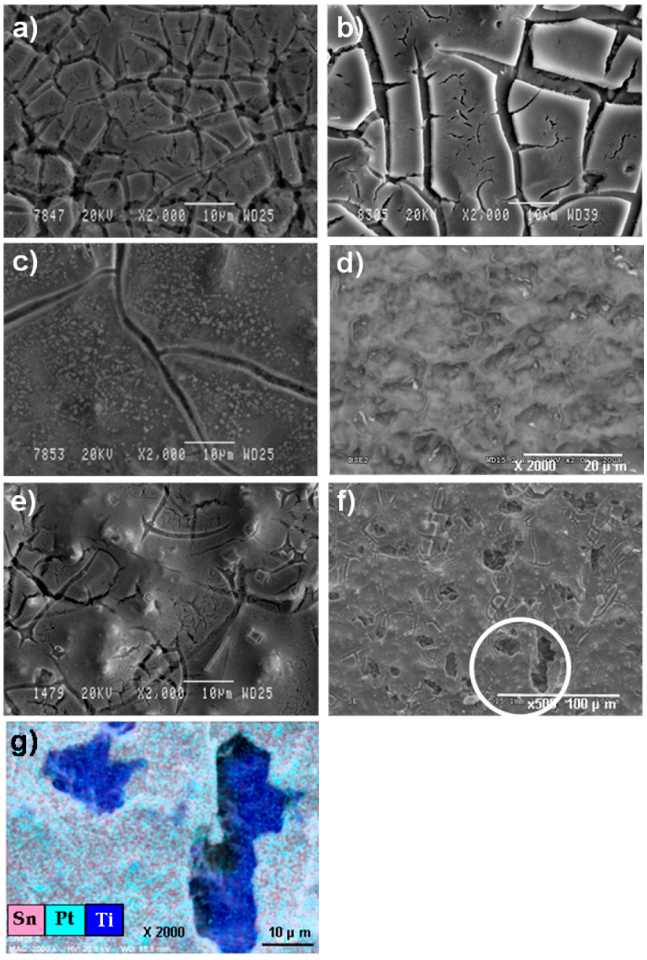

Figure 1. SEM images of (a) fresh SnO_2–Sb/Ti electrode, (b) deactivated SnO_2–Sb/Ti electrode, (c) fresh RuO_2/Ti electrode, (d) deactivated RuO_2/Ti electrode, (e) fresh SnO_2–Sb–Pt/Ti electrode, (f) deactivated SnO_2–Sb–Pt/Ti electrode, and (g) EDX-mapping of the circled area in f.

the typical cracked-mud morphology of these metal oxide coatings prepared by thermal decomposition.[20,21,28,35] These surface cracks may be produced during the electrode cooling to room temperature[20,28] and/or by solvent evaporation during heating stages.[36] Nevertheless, the incorporation of a small amount of Pt (3 at. %) in the SnO_2–Sb layer (Figure 1e) significantly reduces the number of cracks and pores, producing a compacting effect that has been attributed to a strengthening and shortening of the oxide intercolumn bondings caused by Pt aggregates on the surface of SnO_2 grains.[37]

The surface cracks on the SnO_2–Sb-Pt/Ti oxide layer disappear and porosity dramatically increases upon substituting Sb with 3.25 at. % Ru in the nominal composition (Figure 2a).

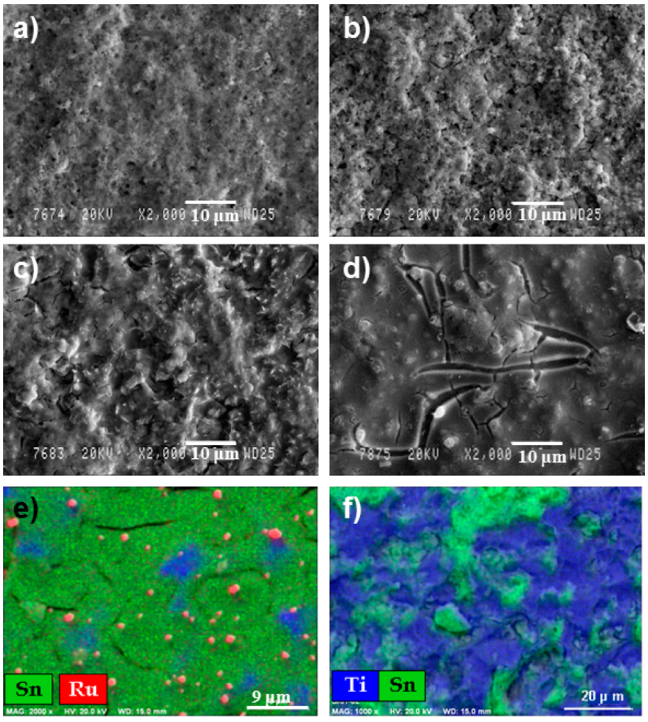

Figure 2. SEM images of fresh SnO_2–Sb(13–x)–Pt–Ru(x)/Ti electrodes with (a) x = 3.25 at. % (Ru), (b) x = 6.50 at. % (Ru), (c) x = 9.75 at. % (Ru), (d) x =13.00 at. % (Ru), (e) fresh SnO_2–Ru/Ti electrode; and deactivated SnO_2–Sb(13–x)–Pt–Ru(x)/Ti electrode; ~~(f)~~ x = 3.25 at. % Ru.

However, further incorporation of Ru (6.50–9.75 at. %) gradually reduces the oxide surface roughness (Figure 2b-c) until the cracked-mud structure is restored again at a ruthenium content of 13 at. % (Figure 2d).[33] In addition, the presence of small grains is also observed in these latter electrodes (Figure 2d). The EDX mapping shows that the small grains contain a high concentration of Ru, indicating phase separation. The phase separation/segregation of Ru in Sn–Ru mixed oxides synthesized by traditional methods has been reported in the literature.[38–40]

3.1.2. Chemical Composition. EDX spectra and mappings registered at different regions of the electrode surfaces showed a homogeneous distribution of the elements in the oxide films. The low signals from the underlying Ti evidenced that a good coverage of the substrate was achieved. According to the methodology reported elsewhere,[28,33] the coating thickness estimated from oxide loadings ranged between 2 and 3 μm. The nominal and experimental compositions of the different mixed metal oxides were expressed as the amount of individual metals with respect to the total metal content, M, (atomic ratios) (Table 2). Comparisons between bulk and surface compositions, obtained by EDX and XPS analysis, respectively, provided some insight into the distribution of the different species. The fairly good correlation between the nominal and EDX experimental Sn/M and Sb/M ratios in SnO_2–Sb/Ti and SnO_2–Sb-Pt/Ti (x = 0.00%) electrodes points out that Sn and Sb were successfully combined in the desired proportions, although Sb depletion occurs at the surface of these electrodes.

Table 2. Nominal and Experimental EDX and XPS Atomic Ratios with Respect to the Total Metal Content (M) Obtained for Fresh And Deactivated (Deact.) Electrodes

electrode	x	Sn/M[a]			Sb/M			Pt/M			Ru/M			I_{OH}/I_{OM}[b]	
		nom.	EDX fresh	XPS fresh	XPS deact	nom.	EDX fresh	XPS fresh	XPS deact	nom.	EDX fresh	XPS fresh	XPS deact	XPS fresh	XPS deact
SnO_2−Sb/Ti		0.87	0.88	0.94	0.92	0.13	0.12	0.06	0.07					0.27	0.12
SnO_2−Sb(13−x)−Pt−Ru(x)/Ti	0.00	0.84	0.83	0.88	0.90	0.13	0.11	0.07	0.05	0.03	0.06	0.04	0.06	0.24	0.18
	3.25	0.84	0.69	0.66	0.73	0.10	0.24	0.32	0.10	0.03	0.04	0.02	0.17	0.54	0.34
	6.50	0.84	0.69	0.71	0.79	0.06	0.19	0.21	0.07	0.03	0.05	0.06	0.14	0.32	0.27
	9.75	0.84	0.72	0.90	0.85	0.03	0.10	0.05	0.09	0.03	0.06	0.03	0.06	0.23	0.12
	13.00	0.84	0.78	0.96	0.87					0.03	0.06	0.02	0.11	0.27	0.30
SnO_2−Ru/Ti		0.87	0.79	0.96	0.98					0.13	0.16	0.02	0.13	0.55	0.26
RuO_2/Ti										1.00	1.00	1.00	1.00	0.00	0.74

[a]Total metal content, M = Sn + Sb + Pt + Ru. [b]Adsorbed oxygen O−H (OAds.) to oxide-lattice oxygen M−O (Ooxid.) photoemission intensities ratio (corrected values from deconvoluted O(1s), C(1s), and Ti(2p-XPS spectra): IOH = [OAds.] − [C−OH] and IOM = [Ooxid.] − 2[Ti].

In the same manner, the similarity between nominal and EDX-obtained Ru/M ratios shows that the amount of Ru introduced in the SnO_2−Sb(13−x)−Pt−Ru(x)/Ti electrodes approaches quite well the desired one, whereas the surface Ru content (XPS ratio) remains almost constant and much lower than the nominal one (Figure 3a). As shown in Figure 3b and Table 1, the introduction of a low Ru content (x = 3.25 at. %) produces a marked enrichment in Sb and a marked depletion in Sn, in both the bulk and the surface of the electrodes. A further increment in the Ru content gradually increases the Sn/M ratio and reduces the Sb/M ratio to values (for x = 9.75 at. %) closer to those obtained in the absence of Ru (x = 0.00 at. %) (Table 1). On the other hand, the comparison among the nominal and EDX and XPS experimental Ru/Sb ratios (Figure 3c.) shows that only about one-third of Sb is replaced by Ru. This may indicate that Ru does not effectively replace Sb in the mixed oxide, but it may replace Sn in the rutile-like lattice, hence explaining its depletion. Finally, the amount of Pt (bulk) introduced in the coatings is above (almost double) the nominal one, regardless of the Ru content (Table 1), whereas the Pt surface content varies above and below the nominal one with no clear trend. However, a clear surface depletion of Ru with respect to both its nominal and experimental bulk values is observed in the whole set of SnO_2−Sb(13−x)-Pt(3)−Ru(x)/Ti electrodes.

3.1.3. Surface Chemical State. The Sn(3d) spectra of the different SnO_2-based electrodes (Figure 4a) show two peaks at 487.0 and 495.4 eV, typically assigned to the Sn $3d_{3/2}$ and $3d_{5/2}$ states from the spin−orbital splitting,[41,42] which may correspond to either SnO, SnO_2 or $Sn(OH)_x$ species.[41,42] Since the XPS spectrum (not shown) does not exhibit any Sn(5s) peak attributed to SnO, the Sn(3d) signals are assigned to SnO_2.[41] In agreement with data previously reported,[43] the incorporation of low Pt doping levels in mixed Sn−Sb oxides (Figure 4a, x = 0.00%) does not produce any change neither in the Sn(3d) core-level binding energy nor in their energy width and symmetry with respect to undoped materials. This result suggests that the electronic structure of the SnO_2 lattice is unaffected by Pt atoms at such a low content.[41] The Pt $4f_{7/2}$ core level photoemission peak observed for the SnO_2−Sb(13−x)−Pt-Ru(x)/Ti electrodes can be separated into three main contributions and three satellite peaks (Figure 4c). These peaks are associated with the presence of metallic platinum (Pt(0)) and Pt(II) and Pt(IV) species), and their relative concentration was found to vary randomly among the different electrodes.[43]

On the other hand, the XPS spectra in the energy region between 525 and 544 eV revealed the presence of another two peaks (Figure 4d). The peak at 540 eV corresponds to the Sb $3d_{3/2}$ signal, while that at 531 eV is composed of the O(1s) (at 531 eV) together with the Sb $3d_{5/2}$ signals. The deconvolution of the Sb $3d_{3/2}$ signal revealed that the largest fraction of Sb in the SnO_2−Sb/Ti electrode has a 5+ oxidation state (contribution at 530.6 eV[28,43−46]), although Sb(III) (22 at. %) was also observed in this electrode.[41,46] Some authors have indicated that Sb(III) is preferentially located on the surface and grain boundaries of the SnO_2−Sb film.[41,46] On the contrary, the Sb $3d_{3/2}$ peak in SnO_2−Sb(13-x)−Pt-Ru(x)/Ti electrodes (Figure 4d) can be satisfactorily fitted with a single photoemission contribution corresponding to Sb atoms in a 5+ charge state (usually represented as SnO_2−Sb_2O_5). This is in agreement with the results of Montilla et al.,[43] who found that the presence of a small Pt content on the electrode surface promotes the complete oxidation of Sb in the oxide coating.

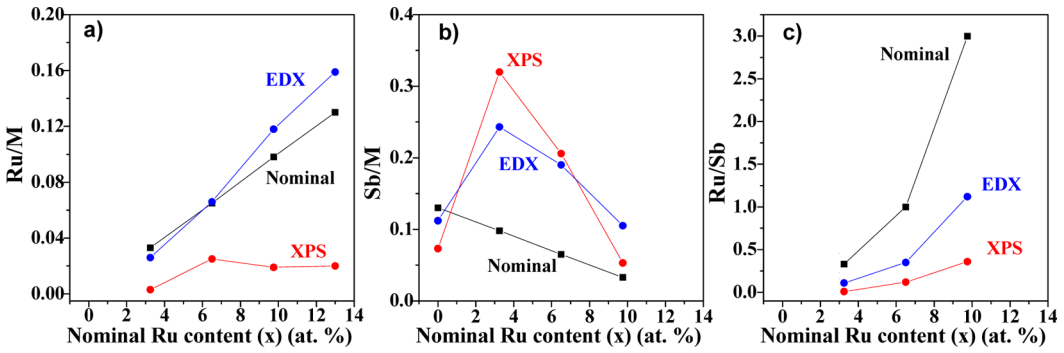

Figure 3. EDX and XPS atomic ratios relative to the total metal content (M) of SnO_2−Sb(13−x)−Pt−Ru(x)/Ti electrodes as a function of the nominal Ru content: (a) Ru/M; (b) Sb/M, and (c) Ru/Sb.

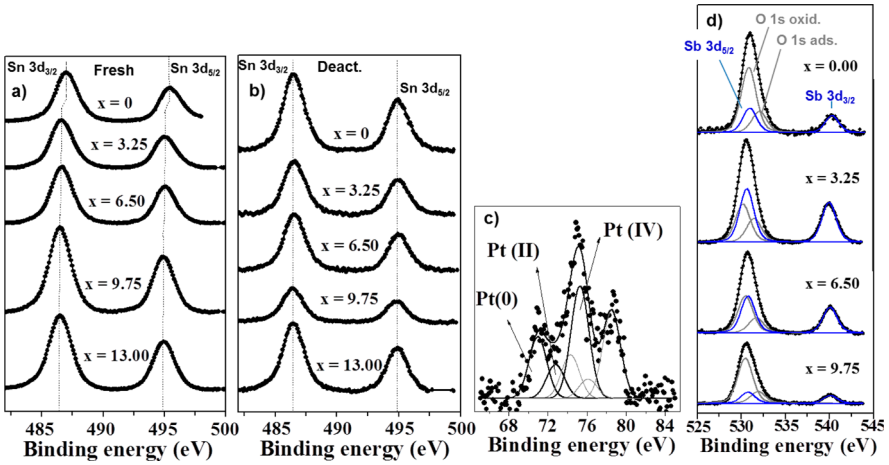

Figure 4. Sn(3d) XPS spectra of (a) fresh SnO_2−Sb(13-x)−Pt-Ru(x)/Ti electrodes, (b) deactivated SnO_2−Sb(13−x)−Pt−-Ru(x)/Ti electrodes; (c) Pt(4f) XPS spectrum of a fresh SnO_2−Sb−-Pt/Ti electrode; and (d) Sb(3d) XPS spectra of fresh SnO_2−Sb(13−x)−Pt-Ru(x)/Ti electrodes.

With the theoretical peak intensity ratio and splitting of the Sb(3d) spin−orbit doublet (1.44 and 10.7 eV, respectively), we used the Sb $3d_{3/2}$ peak to correct the O(1s) photoemission line from the Sb $3d_{5/2}$ interference.[43,45] After the correction, the O(1s) signal could be deconvoluted into two peaks (Figure 4d). The major peak at 530.9 eV is associated with oxygen directly bonded to a metal atom (metal oxides) and the minor one (532.1 eV) is related to oxygen bonded to metal hydroxides or hydrated species on the surface.[41,43]

The introduction of Ru (SnO_2−Sb(13−x)−Pt-Ru(x)/Ti electrodes) leads to the appearance of Ru $3d_{5/2}$ and $3d_{3/2}$ peaks at 282.3 and 284.8 eV, respectively, which overlap with the region of C(1s) core level spectra of adventitious carbon (Figure 5a). These two peaks are observed also in the spectrum of pure RuO_2/Ti electrode (Figure 5b) and are assigned to ruthenium(IV) oxide.[47] Moreover, the progressive substitution of Sb by Ru in the nominal composition causes a band shift of Sn $3d_{5/2}$ and $3d_{3/2}$ peaks toward lower binding energies (Figure 4a), whereas it does not cause a significant effect on the binding energy of Sb $3d_{3/2}$ and O(1s) (Figure 4d). These results may indicate that there is no interaction between Sb and Ru species, but instead, a strong chemical interaction between Sn(IV) and Ru(IV) cations occurs.

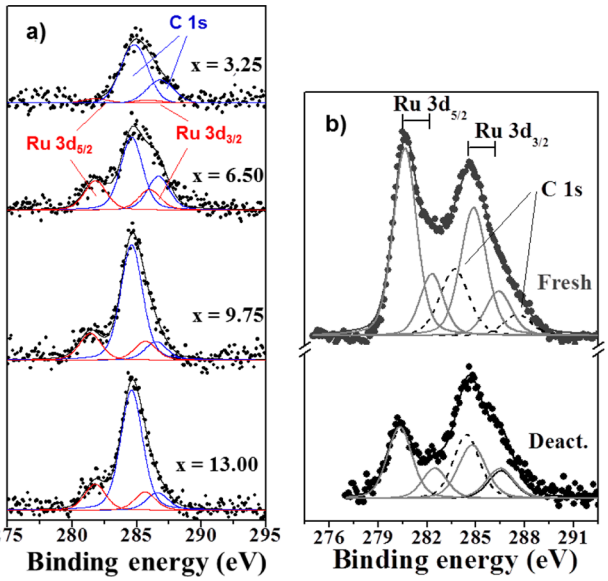

Figure 5. Ru(3d) XPS spectra of (a) fresh SnO_2−Sb(13−x)−Pt−Ru(x)/Ti electrodes and (b) fresh and deactivated RuO_2/Ti electrodes.

3.1.4. Structural Characterization. Figure 6a shows the XRD diffraction patterns of the as-prepared SnO_2−Sb(13−x)−Pt−Ru(x)/Ti electrodes. For comparison purposes, the XRD diffraction peaks of RuO_2 and the Ti substrate are also included in this figure. The XRD diffractogram of the SnO_2−Sb-Pt/Ti electrode is very similar to that of SnO_2−Sb/Ti (see Figure S2 in the Supporting Information) with sharp peaks corresponding to the tetragonal rutile-like structure of SnO_2 cassiterite.[44] In a similar way, the observed XRD of the RuO_2/Ti electrode

dx.doi.org/10.1021/am506958k | ACS Appl. Mater. Interfaces XXXX, XXX, XXX−XXX

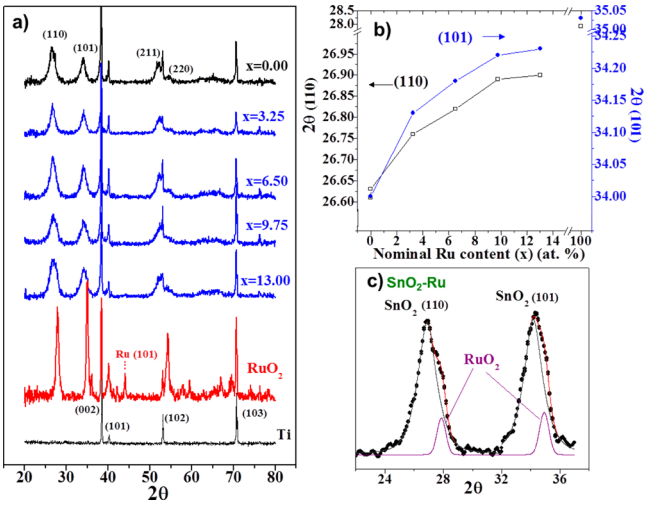

Figure 6. (a) X-ray diffraction patterns of fresh SnO_2−Sb(13−x)−Pt−Ru(x)/Ti electrodes and RuO_2/Ti electrode; (b) (110) and (101) peak position as a function of the nominal Ru content; (c) deconvolution of (110) and (101) peaks for SnO_2−Ru/Ti electrode.

Table 3. Lattice Parameters (a = b and c) of the Rutile-like Structure, Unit-Cell Volume (V), and Crystallite Size (d_c) for the As-Prepared Electrodes Calculated from XRD Patterns

electrode	x	a (Å)[b]	c (Å)[b]	V (Å^3)[b]	d_c[c] (nm)
SnO_2, cassiterite[a]		4.740	3.190	71.7	
SnO_2−Sb/Ti		4.734	3.173	71.1	5.6
SnO_2−Sb(13−x)−Pt−Ru(x)/Ti	0.00	4.730	3.173	71.0	5.7
	3.25	4.708	3.161	70.1	5.8
	6.50	4.697	3.154	69.6	5.5
	9.75	4.687	3.152	69.2	5.2
	13.00	4.685	3.147	69.1	5.2
SnO_2−Ru/Ti		4,685	3.148	69.1	5.5
RuO_2/Ti		4.504	3.113	63.1	13.2
RuO_2[a]		4.499	3.107	62.9	

[a]JCPS-International Centre for Diffraction Data. [b]Lattice parameters were calculated with the Bragg's equation. [c]Average crystallite size determined from (110), (101), (211), and (220) SnO_2-phase reflections and Scherrer's equation. The width of the deconvoluted SnO_2 phase reflection was considered where segregation of RuO_2 occurs.

(Figure 6a) is also in agreement with the tetragonal rutile-like structure of RuO_2 (Table 2). The replacement of Sb by Ru in the nominal composition does not result in the appearance of new diffraction peaks. However, the progressive incorporation of Ru into the oxide coating shifts the SnO_2 diffraction peaks to higher Bragg angles, although this increase is small above x = 9.75 at. % (Figure 6b). As it is shown in Table 2, the increase in Bragg angles involves a gradual reduction in the unit-cell parameters and, consequently, in the volume of the unit-cell. This indicates that Ru(IV), which has a smaller ionic radius than Sn(IV) (0.76 Å against 0.83 Å), is incorporated into the cationic SnO_2 sublattice to form a solid solution $(Ru_\delta Sn_{1-\delta})O_2$, leading to the contraction of the rutile-like lattice.[39,47,48] The formation of such a solid solution is strongly supported by the marked effect of Ru in the Sn(3d) binding energies (Figure 4a) . Nevertheless, the diffraction peaks for x = 9.75 at. % start to display certain asymmetry that becomes more important at the highest Ru content. This asymmetry is more noticeable in the SnO_2−Ru/Ti electrode prepared in the same conditions (Figure 6c). The deconvolution of these diffraction peaks reveals that the asymmetry corresponds to the formation of a RuO_2 phase. Both the appearance of peak asymmetry and the leveling off in the Bragg angle shift from x = 9.75 at. % suggest that the mixed oxide reaches the solubility limit of Ru cations into the rutile-like SnO_2 lattice, so Ru starts to segregate as RuO_2 phase.

In spite of the structural changes, Table 3 shows that the addition of the doping metals like Ru, Sb or Pt, produces almost no effect in the average crystallite size of the different oxides, which ranges between 5.2 and 5.8 nm. This crystallite size is in agreement with the average particle size (around 5−10 nm), observed by TEM (Figure 7). The figure includes TEM images of SnO_2−Sb(13−x)−Pt−Ru(x) oxides with different Ru contents. The oxides consist of highly aggregated particles with ellipsoidal-like morphology, in agreement with other transition metal oxides prepared by thermal decomposition.[49] In particular, specific phases characteristic of Sb, Pt, and Ru dopants were not distinguished, in accordance with XRD results, and the lack of significant differences among the three images reveals that the introduction of Ru in the mixed solid solution $(Ru_\delta Sn_{1-\delta})O_2$ causes practically no effect in the microstructure of the oxides.

3.2. Electrochemical Measurements. *3.2.1. Electrochemical Behavior.* Figure 8 shows the voltammetric response of the as-synthesized electrodes in alkaline medium. The voltammogram of SnO_2−Sb/Ti electrode (Figure 8a) shows no oxidation/reduction peaks and a sharp current rise, corresponding to the oxygen evolution reaction (OER), at potentials above 1.8 V. These features are common to nonactive oxides. In the presence of Pt (x = 0.00 at. %) (Figure 8b), the onset of the OER is shifted to lower potentials (around 1.7 V) and the voltammogram includes a broad oxidation peak (between 0.7 and 1.4 V) and a much better-defined reduction counterpart (at ca. 0.65 V) attributed to the formation and reduction of surface platinum oxides (Pt/PtO_x) (A_1/C_1).[28]

The gradual introduction of Ru in SnO_2-based electrodes (Figure 8c−h) results in the appearance of various redox couples associated with the surface transitions of Ru in RuO_2 electrodes (Figure 8h): (i) Ru(II) ↔ Ru(III) (A'_1/C'_1), (ii) Ru(III) ↔ Ru(IV) (A'_2/C'_2), (iii) Ru(IV) ↔ Ru(VI) (A'_3/C'_3) and (iv) Ru(VI) ↔ Ru(VII) (A'_4/C'_4).[47,50] The current of these peaks increases with the Ru content. Furthermore, the onset potential of OER is shifted by about 0.1 V to less positive potentials than the observed for SnO_2−Sb-Pt/Ti electrode because of the electrocatalytic effect of Ru on the OER.

The capacitance of the electrodes in 0.1 M NaOH was measured at different potentials (Table 4) by cyclic voltammetry at various scan rates according to a previously reported procedure.[28,33,51] The capacitance of SnO_2−Sb/Ti and SnO_2−Sb−Pt/Ti (x = 0.00 at. %) electrodes in alkaline electrolyte decreases with the potential, showing the characteristic behavior for a n-type semiconductor, whereas that of the RuO_2/Ti electrode increases with the potential, characteristic of p-type semiconductors. The effect of Ru incorporate in SnO_2−Sb(13−x)−Pt−Ru(x)/Ti electrodes is manifested by an increase in capacitance even for low Ru content. These results highlight the marked effect of Ru on the electrochemical response of SnO_2-based electrodes in alkaline conditions.

The capacitance values provide information on the real, electrochemically active, surface area of the electrodes through the so-called roughness factor (Rf), which is defined as the real

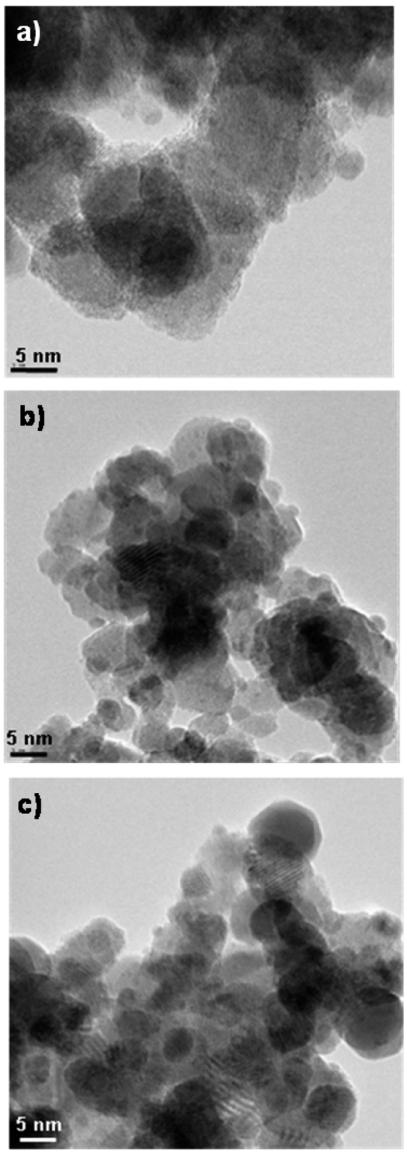

Figure 7. TEM images of fresh SnO_2−Sb(13−x)−Pt−Ru(x)/Ti electrodes: (a) x = 0.00 at. % Ru; (b) x = 6.50 at. % Ru; (c) x = 9.75 at. % Ru.

surface area per geometric area of electrode (2 cm^2) and is one of the electrocatalytic activity-determining factors. The values of Rf were estimated from the experimental capacitance values at 0.55 V and the specific capacitance of SnO_2-based (8 μF cm^{-2})[52] and RuO_2 (80 μF cm^{-2})[53] electrodes. The introduction of Ru (Figure 9a) produces an increase in the roughness factor at 0.55 V and the different voltammetric charges of the SnO_2−Sb(13−x)−Pt−Ru(x)/Ti electrodes, reaching a maximum when x = 3.25 at. %,. Then these parameters slightly decrease with the increase in Ru content.

The voltammetric charge (q^*) is another important parameter influenced by both the real surface area (geometric factors) and the specific electroactivity of the sites, which depends on the chemical composition of the oxide layers (electronic factors). The total (q_{TOT}^*), outer (q_{OUT}^*), and inner (q_{IN}^*) voltammetric charges of the electrodes were measured by using the procedure described in the literature.[51] These charges are related to the total, the most accessible and the less accessible (pores, cracks, grain boundaries, etc.)[48] electroactive surface, respectively (Figure 9a). These electrical charges show the same tendency as roughness factor. The so-called electrochemical porosity (P_e) (Table 3), obtained from the inner charge to total charge ratio (q_{IN}^*/q_{TOT}^*) also shows the same tendency.[28,48] These trends are in good agreement with the morphology changes observed by SEM and suggest that, unlike in acid medium,[33] the electrochemical response of these electrodes in NaOH solution is governed by geometric factors (i.e., by the surface area exposed to the electrolyte solution).

3.2.2. Oxygen Evolution Reaction (OER). The electrocatalytic activity of the different electrodes in alkaline medium was evaluated from the linear region of their corresponding Tafel plots (log j vs E)[54] (see the Supporting Information, Figure S3). The Tafel slopes provide relevant information on reaction mechanisms, whereas the y-intercept of the Tafel plot at j = 0 is related to the exchange current density (j_0), i.e. the intrinsic ability of an electrocatalyst to catalyze a reaction at η = 0 V.[54] Thus, the lower the y-intercept value (b in Figure 9b), the higher j_0. As shown in Figure 9b, SnO_2−Sb/Ti and SnO_2−Sb−Pt/Ti (x = 0) electrodes exhibit a Tafel slope in alkaline conditions of around 120 mV dec^{-1}, which suggests a kinetic control by the adsorption of OH^- according to the generally proposed OER mechanism.[54] These Tafel slopes, together with the high values of y-intercept constant ($b \approx$ 2.4 V, Figure 9b), are in close agreement with those found in the literature for SnO_2-based electrodes[28,48] and reflect their poor electrocatalytic activity toward the OER. As the Ru content in the oxide layer increases, the values of both constants decrease down to 80 mV dec^{-1} and 1.8 V, respectively, for x = 13.0 at. % electrodes, approaching to those of RuO_2/Ti (~40 mV dec^{-1} and $b \approx$ 1.6 V). These low values are typical of RuO_2 anodes and involve the electro-oxidation of the intermediate surface complex as the rate-determining step and a high electrocatalytic activity for the OER in these conditions. Thus, the decrease in Tafel constants indicates that the introduction of Ru in SnO_2−Sb−Pt/Ti electrodes gradually increases the electrocatalytic activity of the electrodes toward the OER, with a weakening of the metal−oxygen bond strength on the surface and a modification of the rate-determining step. A similar electrocatalytic effect for Ru in SnO_2−based anodes was also observed by other authors in both acidic[33,48] and alkaline[55] media. From Tafel results, it is suggested that the first step becomes more facilitated when Sb is replaced by Ru because of its higher redox activity, the induced change in the charge carrier mechanism, an increase in its electrical conductivity[48] and its exceptional ability to form hydrated oxides through the following mechanism[51]

$$RuO_x(OH)_y + \delta H_2O + \delta e^- \leftrightarrow RuO_{x-\delta}(OH)_{y+\delta} + \delta OH^- \quad (1)$$

3.3. Electrode Stability and Deactivation Mechanism. *3.3.1. Electrode Stability.* Figure 9c depicts the evolution of the electrode potential with the electrolysis time upon anodic polarization at 0.5 A cm^{-2} in 1 M NaOH. The electrode potential remains stable for a certain period of time, the so-called service life, until it undergoes a sharp rise indicating deactivation. Table 3 summarizes the service life of the different electrodes, expressed as efficiency. The obtained results highlight the extremely short and long service life of the SnO_2−Sb and RuO_2 electrodes in 1 M NaOH, respectively. Particularly, the value for SnO_2−Sb is even much shorter than those reported for the deactivation process of Sb-doped SnO_2

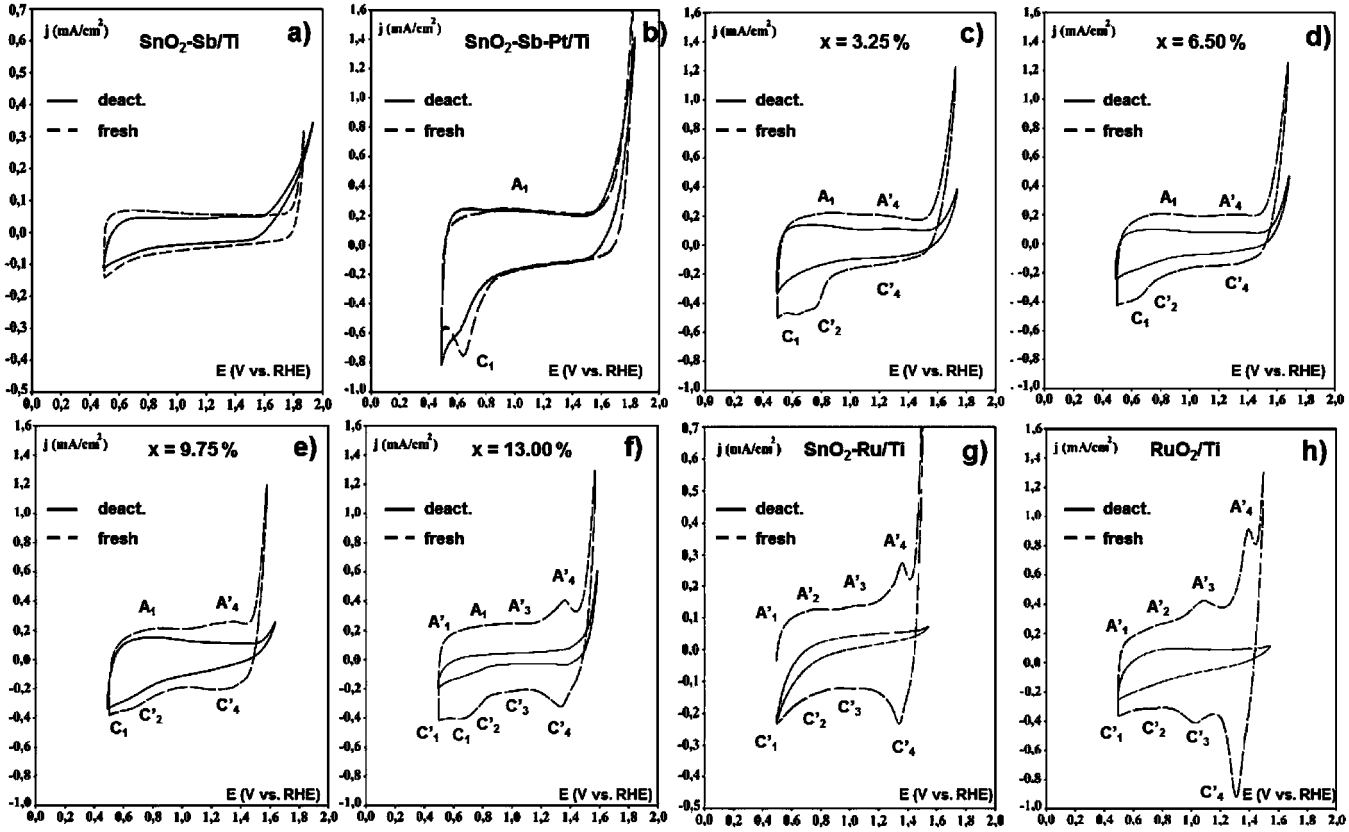

Figure 8. Steady cyclic voltammograms of fresh and deactivated electrodes in a 0.1 M NaOH solution, (a) SnO_2−Sb/Ti electrode, SnO_2−Sb(13−x)−Pt−Ru(x)/Ti electrodes with (b) x = 0.00 at. %, (c) x = 3.25 at. %, (d) x = 6.50 at. %, (e) x = 9.75 at. %, (f) x = 13.00 at. %, (g) SnO_2−Ru/Ti electrode, and (h) RuO_2/Ti electrode; v = 20 mV s^{-1}.

Table 4. Service Life (SL) and Service Life Efficiency (SLE), Specific Capacitance, Roughness Factor (Rf), and Electrochemical Porosity (P_e) for the As-Prepared Electrodes in 0.1 M NaOH Solution[a]

				specific capacitance (mF cm^{-2})						
electrode	x	SL (h)	SLE (A h mg^{-1})	0.55 V	0.75 V	0.95 V	1.15 V	1.35 V	Rf at 0.55 V	P_e nom.
SnO_2−Sb/Ti		0.6	0.2	3.1	2.6	2.4	2.1	2.0	389	0.09
SnO_2−Sb(13−x)−Pt−Ru(x)/Ti	0.00	72	22	3.7	3.4	3.0	2.7	2.5	464	0.34
	3.25	189	63	7.4	7.3	6.7	6.1	5.9	931	0.33
	6.50	210	75	7.2	7.2	6.7	6.3	6.3	900	0.32
	9.75	212	106	6.9	7.0	6.7	6.6	7.1	863	0.29
	13.00	86	25	6.1	6.1	5.4	5.9	8.5	761	0.21
SnO_2−Ru/Ti		116	35	3.4	3.5	3.5	3.6	8.6	450	0.10
RuO_2/Ti		640	181	6.8	7.5	8.5	12.1	20.7	85	0.19

[a]Service life (SL) and service life efficiency (SLE, total charge passed per unit mass of deposited oxide) at 0.5 A cm^{-2} in 1 M NaOH solution. The rest of parameters were obtained from voltammetric measurements in 0.1 M NaOH.

electrodes in acidic media.[21,28] By contrast, the stability of RuO_2 in alkaline conditions is much higher than in acid electrolytes (1−3 h).[56]

The introduction of a small amount of Pt (3 at. %) in SnO_2−Sb produces a remarkable stabilizing effect, so that the service life is increased by 2 orders of magnitude (Table 3). Similar service lifes in alkaline medium were observed by Adams et al.,[31] by introducing Pt in SnO_2−Sb_2O_5 electrodes, but using milder anodic polarization conditions (0.16 A cm^{-2} and 0.5 M NaOH) and larger Pt contents (PtO_x (10 wt %)). Nevertheless, the service life of these electrodes in alkaline medium is still lower than that in acid conditions, in which Pt was found to cause proportional stabilizing effects.

The substitution of Sb by Ru in the nominal composition causes an increase in the service life of SnO_2−Sb/Ti and SnO_2−Sb−Pt/Ti electrodes in alkaline conditions. In the presence of Pt, the introduction of Ru increases the service life by up to 1 order of magnitude for the 9.75 at. % electrode. To the knowledge of the authors, the only study on the stability of binary (Sn−Ru)O_2 oxides in alkaline conditions was carried out by Lyons and Burke,[57] who obtained a maximum service life of 240 h in stronger conditions (6 M NaOH; 0,75 A cm^{-2} and 80 °C) for a thicker electrode (4 mg cm^{-2}) with 40% RuO_2. In terms of efficiency, the service life (SLE) of these electrodes (45 Ah mg^{-1}) was considerably lower than those found in this work for Pt- and Ru-doped SnO_2 anodes (63−106 A h mg^{-1}) (Table 3), by using even about 4−12 times higher Ru contents

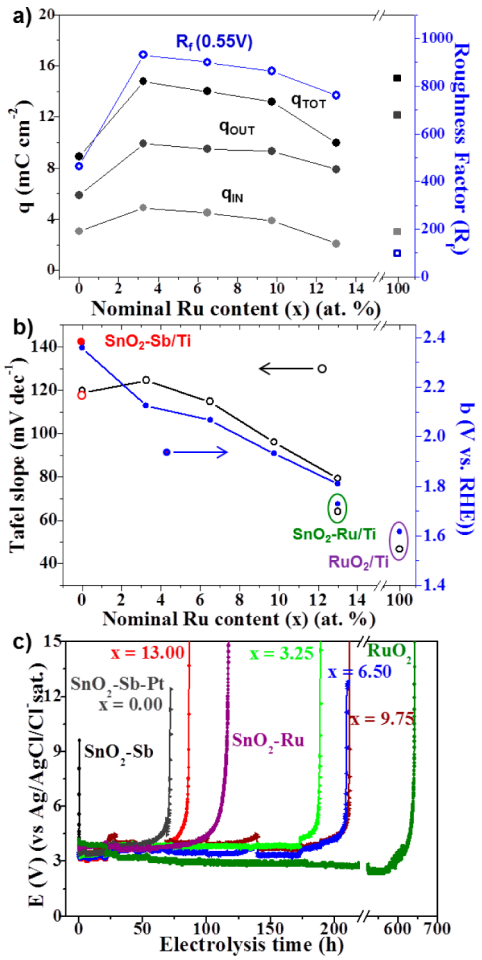

Figure 9. (a) Total (q_{TOT}), outer (q_{OUT}), and inner (q_{IN}) charges and roughness factor for the SnO_2−Sb(13−x)−Pt−Ru(x)/Ti electrodes and RuO_2/Ti electrode as a function of the nominal Ru content; (b) Tafel slope and Tafel line y-intercept as a function of the nominal Ru content; and (c) potential vs electrolytsis time during service life tests for the different electrodes indicated in the figure.

in the former case. The highest stabilities obtained by combining low amounts of Pt (3%) and Ru (3.25−6.50 at. %) highlights the outstanding synergistic effect of Pt and Ru in these quaternary SnO_2−Sb(13−x)−Pt-Ru(x)/Ti mixed oxides. Several strategies have been used in order to improve the service life of these types of electrodes. Recently, the introduction of carbon nanotubes (CNT) in the Ti/SnO_2−Sb-CNT composition increases the service life 4.8 times compared to the Ti/SnO_2−Sb electrode, showing a superior electrochemical oxidation and degradation abilities for organic pollutants.[30]

3.3.2. Characterization of Deactivated Electrodes. Although a little more cracked and deteriorated, the surface texture of the deactivated SnO_2−Sb electrode (Figure 1b) is rather similar to that of the fresh ones (Figure 1a), whereas the deactivated SnO_2−Sb-Pt electrode additionally exhibits the detachment of some regions of the oxide coating throughout the whole surface (Figure 1f) exposing the Ti substrate to the electrolyte (Figure 1g). In RuO_2/Ti electrodes, the anodic polarization process produces the detachment of almost the whole RuO_2 layer and only some small fragments remain attached to the support surface after deactivation (Figure 1d). On the other hand, and independently of the Ru content, deactivated SnO_2−Sb(13−x)−Pt−Ru(x)/Ti and SnO_2−Ru/Ti electrodes showed a more pronounced detachment of the oxide layer than in the case of SnO_2−Sb−Pt/Ti electrode, with small coating fragments but less marked than that of RuO_2/Ti. The Sn/M ratio is practically maintained in the deactivated electrodes; however, the Sb/M and Ru/M ratios decrease (Table 1), and the Pt/M increases.

The partial detachment of the outer or a localized-region of the SnO_2-based oxide layers was evidenced by (i) the presence of Sn, Sb, and Pt in the used alkaline electrolytes (even in the case of SnO_2−Sb), as determined by ICP analysis; (ii) the appearance or increase of Ti signal in XPS or EDX and XRD results (see Figure S2 in the Supporting Information). In spite of the damage of the outer surface layers, XPS revealed that the anodic polarization does not modify the binding energies of Sn(3d), Sb(3d) and O(1s) core levels (Figure 4) of the deactivated electrodes, although metallic Pt completely transforms into oxidized Pt (II) and Pt (IV) species (see Figure S1a in the Supporting Information).[43] Moreover, XRD patterns of deactivated electrodes still keep the characteristic rutile-like structure.

The detailed analysis of core level photoelectron spectra of the different deactivated SnO_2-based electrodes show a decrease in the I_{OH}/I_{OM} ratios (Table 1), indicating a higher relative increase in the amount of oxygen atoms bonded to metal (OM). Moreover, the effect of Ru content in the binding energies of Sn $3d_{3/2}$ and $3d_{5/2}$ states of the different Ru-doped SnO_2 electrodes, disappears after deactivation (Figure 4b). Also their voltammograms show a dramatic loss of the voltammetric charge and do not exhibit the characteristic redox peaks of Ru species within the entire potential range (Figure 8c-h). The onset of the OER is also shifted to more positive potentials.

The similarity between the surface Sn/M atomic ratio of fresh and deactivated SnO_2−Sb and SnO_2−Sb−Pt electrodes, determined by XPS (Table 1), together with the general decrease in the corrected I_{OH}/I_{OM} ratios, seem to rule out the formation of a passivating surface layer of tin hydroxides ($Sn(OH)_4$) and/or hydrates.[43] These facts reveal that the deactivation mechanism of these electrodes in alkaline conditions is different to that proposed for acid medium.[20,26,43]

On the other hand, the similar voltammetric profile of fresh and deactivated electrodes (Figure 8) indicates that the SnO_2−Sb/Ti and SnO_2−Sb-Pt/Ti deactivated ones preserve the ability to transfer charge across the surface. The OER currents are considerably tilted, especially in the case of SnO_2−Sb/Ti electrodes. This fact may be due to the growth of a TiO_2 interlayer.[58] In the case of SnO_2−Sb−Pt/Ti the conversion of metallic Pt to Pt(IV) and Pt(II) species can originate a reduction in the number of oxygen vacancies[42] and a decrease of its electrocatalytic activity for OER. Consequently, the deactivation of SnO_2−Sb and SnO_2−Sb−Pt electrodes in NaOH is proposed to occur by a nonselective dissolution of metallic species in alkaline conditions, accompanied by some degree of coating detachment, that allows the NaOH electrolyte to contact and passivate the MO_x/Ti interphase.[59]

The detachment of the whole RuO_2 coating in RuO_2/Ti electrodes was confirmed by the remarkably high Ti/M ratio and the increase of both the Ti(2p) core-level peak (associated with TiO_2)[60] (see Figure S1b in the Suypporting Information) and the relative intensity of Ti diffraction peaks (see Figure S2 in the Supporting Information), as well as the decrease in the Ru(3d) photoelectron peak (Figure 4d), the complete disappearance of RuO_2 diffraction peaks (see Figure S2b in

dx.doi.org/10.1021/am506958k | ACS Appl. Mater. Interfaces XXXX, XXX, XXX−XXX

the Supporting Information) and the absence of Ru redox peaks and extremely low currents in its CV profile (Figure 8h). This may be related to the electrochemical dissolution of RuO_2 in alkaline medium at high potentials,[57] which has been associated with the electrochemical generation of soluble RuO_4^{2-} species during O_2 production

$$(-O-)_2RuO_2(OH)_2 + 2H_2O \leftrightarrow 2(-OH) + RuO_2(OH)_4 \quad (2)$$

$$RuO_2(OH)_4 + 4OH^- \leftrightarrow RuO_4^{2-} + 4H_2O + 2e^- + O_2 \quad (3)$$

From the detailed characterization of fresh and deactivated electrodes, it is proposed that the anodic deactivation of SnO_2–Sb(13–x)–Pt–Ru(x)/Ti electrodes in NaOH electrolyte occurs by a mixed mechanism. Thus, dissolution of metallic species, promoted in alkaline conditions and high potentials, the loss of coating, and the passivation of Ti substrate, by formation of an insulating TiO_2 interlayer, act together. Considering this mechanism and the service life of the different electrodes in NaOH (Table 3), the stabilizing effect of Pt may be attributed to its surface compacting effect, what may hinder the penetration of the electrolyte through the coating, and/or to prevent the generation of surface insulating $Sn(OH)_x$ species[28] and/or Sb^{3+} species, which could be important active sites for oxygen and water adsorption.[61] On the other hand, regarding the similarities in microstructure observed by XRD and TEM, the enhanced stability caused by the progressive substitution of Sb by Ru up to a 9.75 at. % Ru, at which Sn and Ru form a solid solution, together with the decreased stability observed for higher Ru contents (x > 9.75 at. %), for which a RuO_2 phase segregation is observed, allow us to suggest that the formation of a homogeneous $(Ru_\delta Sn_{1-\delta})O_2$ single-phase must be the key factor explaining the high stability of SnO_2–Sb(13–x)–Pt–Ru(x)/Ti electrodes. In addition, the high stability of the highest oxidation states of Ru and Pt in alkaline conditions, at potentials where the OER occurs, may also contribute. In this sense, the Ru-doped SnO_2 electrodes may experience deactivation after the observed selective dissolution of Ru from the $(Ru_\delta Sn_{1-\delta})O_2$ phase, which may bring about the coating detachment and the access of electrolyte to the Ti support. On the other hand, the segregation of RuO_2 phase may promote the generation of crystalline and structural defects, which could facilitate the dissolution of inner metal species and the penetration of NaOH electrolyte.

4. CONCLUSIONS

The introduction of Pt (3 at. %) and the nominal substitution of Sb (13 at. %) by Ru in SnO_2–Sb and SnO_2–Sb–Pt electrodes induce different textural, structural and chemical changes that strongly affect the electrocatalytic activity for the OER and electrochemical stability in alkaline conditions. Although both Pt and Ru are mainly incorporated in the bulk of the SnO_2–Sb(13–x)–Pt–Ru(x) electrodes, they introduce their characteristic redox processes and shift the onset of the OER toward lower potentials. However, while Pt does not alter neither the Sn and Sb contents nor the rutile-like crystalline structure, XPS and XRD analysis have shown that, Ru content lower than 9.75 at. %, Ru(IV) atoms, instead of replacing Sb in the mixed oxides (as it could be expected from the change on nominal compositions), occupy positions of Sn(IV) ions in the cationic sublattice of the rutile-like SnO_2 structure to form a solid solution. In addition, surface segregation of Ru is observed as RuO_2 phase at Ru contents larger than 9.75 at. %.

The deactivation of the different electrodes has been found to occur by passivation of the Ti substrate and/or detachment of the oxide coating promoted by alkaline dissolution of metal species at high potentials. Considering this mechanism, Pt causes a compacting effect on the cracked-mud morphology of the SnO_2–Sb coating that, together with its stability under OER conditions, results an increase in the "accelerated" service life of this electrode by 2 orders of magnitude in alkaline medium. Moreover, the introduction of low amounts of Ru (3.25–9.75 at. %) into the SnO_2 rutile-like structure leads to a 3-fold increase in the service life of SnO_2–Sb–Pt/Ti electrodes. However, a further gain in stability with higher Ru contents is not observed probably because of the mixed metal oxide saturation, which leads to Ru segregation as a RuO_2 phase.

Consequently, the obtained results show that the combination of low amounts of Pt and Ru (below the saturation of $(Ru_\delta Sn_{1-\delta})O_2$ solid solutions) greatly enhances the stability of SnO_2–Sb electrodes in alkaline medium. Although the stability of these electrodes does not reach that observed for pure RuO_2, they constitute cheaper alternatives with a higher OER overpotential as attractive properties for different applications in alkaline medium, such as electro-oxidation of compounds in electrosynthesis and electrochemical degradation of pollutants.

■ ASSOCIATED CONTENT

Supporting Information

Additional XPS, XRD, and Tafel plots information. This material is available free of charge via the Internet at http://pubs.acs.org.

■ AUTHOR INFORMATION

Corresponding Author

*E-mail: morallon@ua.es.

Notes

The authors declare no competing financial interest.

■ ACKNOWLEDGMENTS

The authors thank the MINECO, FEDER, and Generalitat Valenciana for the financial support (MAT2013-42007-P, PROMETEO2013/028 projects).

■ REFERENCES

(1) Trasatti, S. Transition Metal Oxides: Versatile Materials for Electrocatalysis. In *The Electrochemistry of Novel Materials*; Lipkowski, J., Ross, P. N., Eds.; VCH; Weinheim, Germany, 1994; pp 207–295.
(2) Hayfield, P. C. S. Development of the Noble Metal/Oxide Coated Titanium Electrode Part III: Coated Titanium Anodes in Widely Ranging Oxygen Evolving Situations. *Platinum Met. Rev.* **1998**, *42*, 116–122.
(3) Park, S.; Shao, Y.; Liu, J.; Wang, Y. Oxygen Electrocatalysts for Water Electrolyzers and Reversible Fuel Cells: Status and Perspective. *Energy Environ. Sci.* **2012**, *5*, 9331–9344.
(4) McCrory, C. C. L.; Jung, S.; Peters, J. C.; Jaramillo, T. F. Benchmarking Heterogeneous Electrocatalysts for the Oxygen Evolution Reaction. *J. Am. Chem. Soc.* **2013**, *135*, 16977–16987.
(5) Martínez-Huitle, C. A.; Ferro, S. Electrochemical Oxidation of Organic Pollutants for the Wastewater Treatment: Direct and Indirect Processes. *Chem. Soc. Rev.* **2006**, *35*, 1324–1340.
(6) Comninellis, Ch.; Pulgarin, C. Anodic Oxidation of Phenol for Waste-Water Treatment. *J. Appl. Electrochem.* **1991**, *21*, 703–708.
(7) Chen, G.; Hung, Y. T. Electrochemical Wastewater Treatment Processes. In *Advanced Physicochemical Treatment Technologies*; Wang,

L. K., Hung, Y. T., Shammas, N. K., Eds.; Handbook of Environmental Engineering Series 5; Springer−Verlag: New York, 2007; pp 57−106.
(8) Berenguer, R.; Marco-Lozar, J. P.; Quijada, C.; Cazorla-Amorós, D.; Morallón, E. Electrochemical Regeneration and Porosity Recovery of Phenol-saturated Granular Activated Carbon in an Alkaline Medium. *Carbon* **2010**, *48*, 2734−2745.
(9) Berenguer, R.; Marco-Lozar, J. P.; Quijada, C.; Cazorla-Amorós, D.; Morallón, E. Comparison among Chemical, Thermal, and Electrochemical Regeneration of Phenol-Saturated Activated Carbon. *Energy Fuels* **2010**, *24*, 3366−3372.
(10) Lin, H.; Niu, J.; Ding, S.; Zhang, L. Electrochemical Degradation of Perfluorooctanoic Acid (PFOA) by Ti/SnO_2-Sb, Ti/SnO_2-Sb/PbO_2, and Ti/SnO_2-Sb/MnO_2 Anodes. *Water Res.* **2012**, *46*, 2281−2289.
(11) Lin, H.; Niu, J.; Xu, J.; Huang, H.; Li, D.; Yue, Z.; Feng, C. Highly Efficient and Mild Electrochemical Mineralization of Long-Chain Perfluorocarboxylic Acids (C9−C10) by Ti/SnO_2−Sb−Ce, Ti/SnO_2−Sb/Ce−PbO_2, and Ti/BDD Electrodes. *Environ. Sci. Technol.* **2013**, *47*, 13039−13046.
(12) Niu, J.; Bao, Y.; Li, Y.; Chai, Z. Electrochemical Mineralization of Pentachlorophenol (PCP) by Ti/SnO_2−Sb Electrodes. *Chemosphere* **2013**, *92*, 1571−1577.
(13) Simon, P.; Gogotsi, Y. Materials for Electrochemical Capacitors. *Nat. Mater.* **2008**, *7*, 845−854.
(14) Wang, G.; Zhang, L.; Zhang, J. A Review of Electrode Materials for Electrochemical Supercapacitors. *Chem. Soc. Rev.* **2012**, *41*, 797−828.
(15) Sieben, J. M.; Morallón, E.; Cazorla-Amorós, D. Flexible Ruthenium Oxide-Activated Carbon Cloth Composites Prepared by Simple Electrodeposition Methods. *Energy* **2013**, *58*, 519−526.
(16) Tarascon, J. M.; Armand, M. Issues and Challenges Facing Rechargeable Lithium Batteries. *Nature* **2001**, *414*, 359−367.
(17) Trasatti, S. Electrocatalysis: Understanding the Success of DSA. *Electrochim. Acta* **2000**, *45*, 2377−2385.
(18) Vercesi, G. P.; Rolewicz, J.; Comninellis, Ch.; Hinden, J. Characterization of DSA-Type Oxygen Evolving Electrodes. Choice of Base Metal. *Thermochim. Acta* **1991**, *176*, 31−47.
(19) Comninellis, Ch.; Vercesi, G. P. Characterization of DSA-Type Oxygen Evolving Electrodes. Choice of a Coating. *J. Appl. Electrochem.* **1991**, *21*, 335−345.
(20) Stucki, S.; Kotz, R.; Carcer, B.; Suter, W. Electrochemical Waste-Water Treatment using High Overvoltage Anodes. 2. Anode Performance and Applications. *J. Appl. Electrochem.* **1991**, *21*, 99−104.
(21) Correa-Lozano, B.; Comninellis, Ch.; De Battisti, A. Service Life of Ti/SnO_2-Sb_2O_5 Anodes. *J. Appl. Electrochem.* **1997**, *27*, 970−974.
(22) Rodgers, J. D.; Jedral, W. J.; Bunce, N. J. Electrochemical Oxidation of Chlorinated Phenols. *Environ. Sci. Technol.* **1999**, *33*, 1453−1457.
(23) Cañizares, P.; Martínez, F.; Díaz, M.; García-Gómez, J.; Rodrigo, M. A. Electrochemical Oxidation of Aqueous Phenol Wastes Using Active and Nonactive Electrodes. *J. Electrochem. Soc.* **2002**, *149*, D118−D124.
(24) Montilla, F.; Michaud, P. A.; Morallón, E.; Vázquez, J. L.; Comninellis, Ch. Electrochemical Oxidation of Benzoic Acid at Boron-Doped Diamond Electrodes. *Electrochim. Acta* **2002**, *47*, 3509−3513.
(25) Treimer, S. E.; Feng, J.; Scholten, M. D.; Johnson, D. C.; Davenport, A. J. Comparison of Voltammetric Responses of Toluene and Xylenes at Iron(III)-Doped, Bismuth(V)-Doped, and Undoped Beta-Lead Dioxide Film Electrodes in 0.50 M H_2SO_4. *J. Electrochem. Soc.* **2001**, *148*, E459−E463.
(26) Vicent, F.; Morallon, E.; Quijada, C.; Vazquez, J. L.; Aldaz, A.; Cases, F. Characterization and Stability of Doped SnO_2 Anodes. *J. Appl. Electrochem.* **1998**, *28*, 607−612.
(27) Ding, H. Y.; Feng, Y. J.; Lu, J. W. Study on the Service Life and Deactivation Mechanism of Ti/SnO_2-Sb Electrode by Physical and Electrochemical Methods. *Russ. J. Electrochem.* **2010**, *46*, 72−76.
(28) Montilla, F.; Morallón, E.; De Battisti, A.; Vázquez, J. L. Preparation and Characterization of Antimony-Doped Tin Dioxide Electrodes. Part 1. Electrochemical Characterization. *J. Phys. Chem. B* **2004**, *108*, 5036−5043.
(29) Forti, J. C.; Olivi, P.; de Andrade, A. R. Characterisation of DSA®-Type Coatings with Nominal Composition Ti/$Ru_{0.3}Ti_{(0.7-x)}Sn_xO_2$ Prepared Via a Polymeric Precursor. *Electrochim. Acta* **2001**, *47*, 913−920.
(30) Zhang, L.; Xu, L.; He, J.; Zhang, J. Preparation of Ti/SnO_2-Sb Electrodes Modified by Carbon Nanotube for Anodic Oxidation of Dye Wastewater and Combination with Nanofiltration. *Electrochim. Acta* **2014**, *117*, 192−201.
(31) Adams, B.; Tian, M.; Chen, A. Design and Electrochemical Study of SnO_2-based Mixed Oxide Electrodes. *Electrochim. Acta* **2009**, *54*, 1491−1498.
(32) Montilla, F.; Morallón, E.; Vázquez, J. L. Evaluation of the Electrocatalytic Activity of Antimony-Doped Tin Dioxide Anodes Toward the Oxidation of Phenol in Aqueous Solutions. *J. Electrochem. Soc.* **2005**, *152*, B421−B427.
(33) Berenguer, R.; Quijada, C.; Morallón, E. Electrochemical Characterization of SnO_2 Electrodes Doped with Ru and Pt. *Electrochim. Acta* **2009**, *54*, 5230−5238.
(34) Iwakura, C.; Sakamoto, K. Effect of Active Layer Composition on the Service Life of (SnO_2 and RuO_2)-Coated Ti Electrodes in Sulfuric-Acid Solution. *J. Electrochem. Soc.* **1985**, *132*, 2420−2423.
(35) Fachinotti, E.; Guerrini, E.; Tavares, A. C.; Trasatti, S. Electrocatalysis of H_2 Evolution by Thermally Prepared Ruthenium Oxide: Effect of Precursors: Nitrate vs. Chloride. *J. Electroanal. Chem.* **2007**, *600*, 103−112.
(36) De Pauli, C. P.; Trasatti, S. Electrochemical Surface Characterization of IrO_2+SnO_2 Mixed-Oxide Electrocatalysts. *J. Electroanal. Chem.* **1995**, *396*, 161−168.
(37) Matko, I.; Gaidi, M.; Chenevier, B.; Charai, A.; Saikaly, W.; Labeau, M. Pt Doping of SnO_2 Thin Films: A Transmission Electron Microscopy Analysis of the Porosity Evolution. *J. Electrochem. Soc.* **2002**, *149*, H153−H158.
(38) Ito, M.; Murakami, Y.; Kaji, H.; Yohikozawa, K.; Takasu, Y. Surface Characterization of RuO_2-SnO_2 Coated Titanium Electrodes. *J. Electrochem. Soc.* **1996**, *143*, 32−36.
(39) Nanni, L.; Polizzi, S.; Benedetti, A.; De Battisti, A. Morphology, Microstructure, and Electrocatalylic Properties of RuO_2-SnO_2 Thin Films. *J. Electrochem. Soc.* **1999**, *146*, 220−225.
(40) Wang, X.; Deng, F.; Tang, Z.; Wu, B.; Tang, D.; Lin, W. The Nature of Phase Separation in a Ru-Sn-O Ternary Oxide Electrocatalyst. *Phys. Chem. Chem. Phys.* **2013**, *15*, 3977−3984.
(41) Liu, W.; Cao, X.; Zhu, Y.; Cao, L. The Effect of Dopants on the Electronic Structure of SnO_2 Thin Film. *Sens. Actuators, B* **2000**, *66*, 219−221.
(42) Batzill, M.; Diebold, U. The Surface and Materials Science of Tin Oxide. *Prog. Surf. Sci.* **2005**, *79*, 47−154.
(43) Montilla, F.; Morallón, E.; De Battisti, A.; Barison, S.; Daolio, S.; Vázquez, J. L. Preparation and Characterization of Antimony-Doped Tin Dioxide Electrodes. 3. XPS and SIMS Characterization. *J. Phys. Chem. B* **2004**, *108*, 15976−15981.
(44) Montilla, F.; Morallón, E.; De Battisti, A.; Benedetti, A.; Yamashita, H.; Vázquez, J. L. Preparation and Characterization of Antimony-Doped Tin Dioxide Electrodes. Part 2. XRD and EXAFS Characterization. *J. Phys. Chem. B* **2004**, *108*, 5044−5050.
(45) Terrier, C.; Chatelon, J. P.; Roger, J. A.; Berjoan, R.; Dubois, C. Analysis of Antimony Doping in Tin Oxide Thin Films Obtained by the Sol-Gel Method. *J. Sol-Gel Sci. Technol.* **1997**, *10*, 75−81.
(46) Slater, B.; Catlow, C. R.; Gay, D. H.; Williams, D. E.; Dusastre, V. Study of Surface Segregation of Antimony on SnO_2 Surfaces by Computer Simulation Techniques. *J. Phys. Chem. B* **1999**, *103*, 10644−10650.
(47) Rochefort, D.; Daboa, P.; Guay, D.; Sherwood, P. M. A. XPS Investigations of Thermally Prepared RuO_2 Electrodes in Reductive Conditions. *Electrochim. Acta* **2003**, *48*, 4245−4252.
(48) Gaudet, J.; Tavares, A. C.; Trasatti, S.; Guay, D. Physicochemical Characterization of Mixed RuO_2-SnO_2 Solid Solutions. *Chem. Mater.* **2005**, *17*, 1570−1579.

(49) Berenguer, R.; Valdés-Solís, T.; Fuertes, A. B.; Quijada, C.; Morallón, E. Cyanide and Phenol Oxidation on Nanostructured Co_3O_4 Electrodes Prepared by Different Methods. *J. Electrochem. Soc.* **2008**, *155*, K110−K115.
(50) Kim, K. W.; Lee, E. H.; Kim, J. S.; Shin, K. H.; Kim, K. H. Study on the Electroactivity and Non-Stochiometry of a Ru-based Mixed Oxide Electrode. *Electrochim. Acta* **2001**, *46*, 915−921.
(51) Ardizzone, S.; Fregonara, G.; Trasatti, S. Inner and Outer Active Surface of RuO_2 Electrodes. *Electrochim. Acta* **1990**, *35*, 263−267.
(52) Wu, N. L.; Hwang, J. Y.; Liu, P. Y.; Han, C. Y.; Kuo, S. L.; Liao, K. H.; Lee, M. H.; Wang, S. Y. Synthesis and Characterization of Sb-Doped SnO_2 Xerogel Electrochemical Capacitor. *J. Electrochem. Soc.* **2001**, *148*, A550−A553.
(53) Sugimoto, W.; Kizaki, T.; Yokoshima, K.; Murakami, Y.; Takasu, Y. Evaluation of the Pseudocapacitance in RuO_2 with a RuO_2/GC Thin Film Electrode. *Electrochim. Acta* **2004**, *49*, 313−320.
(54) Bard, A. J.; Faulkner, L. R. *Electrochemical Methods*; John Wiley & Sons: New York, 1980.
(55) Consonni, V.; Trasatti, S.; Pollak, F.; O'Grady, W. E. Mechanism of Chlorine Evolution on Oxide Anodes. Study of pH Effects. *J. Electroanal. Chem.* **1987**, *228*, 393−406.
(56) Mattos-Costa, F. I.; de Lima-Neto, P.; Machado, S. A. S.; Avaca, L. A. Characterisation of Surfaces Modified by Sol-Gel Derived $Ru_xIr_{1-x}O_2$ Coatings for Oxygen Evolution in Acid Medium. *Electrochim. Acta* **1998**, *44*, 1515−1523.
(57) Lyons, M. E. G.; Burke, L. D. Mechanism of Oxygen Reactions at Porous Oxide Electrodes. 1. Oxygen Evolution at RuO_2 and $Ru_xSn_{1-x}O_2$ Electrodes in Alkaline-Solution under Vigorous Electrolysis Conditions. *J. Chem. Soc., Faraday Trans. 1* **1987**, *83*, 299−321.
(58) Boodts, J. F. C.; Trasatti, S. Effect of Composition on the Electrocatalytic Activity of the Ternary Oxide $Ru_{0.3}Ti_{0.7-x}Sn_xO_2$. 1. Oxygen Evolution from $HClO_4$ Solution. *J. Electrochem. Soc.* **1990**, *137*, 3784−3789.
(59) Beck, F. Wear Mechanisms of Anodes. *Electrochim. Acta* **1989**, *34*, 811−822.
(60) Hopfengärtner, G.; Borgmann, D.; Rademacher, I.; Wedler, G.; Hums, E.; Spitznagel, G. W. XPS Studies of Oxidic Model Catalysts: Internal Standards and Oxidation Numbers. *J. Electron Spectrosc. Relat. Phenom.* **1993**, *63*, 91−116.
(61) Dusastre, V.; Williams, D. E. Sb(III) as a Surface Site for Water Adsorption on $Sn(Sb)O_2$, and its Effect on Catalytic Activity and Sensor Behavior. *J. Phys. Chem. B* **1998**, *102*, 6732−6737.